HHS Public Access

Author manuscript

Nature. Author manuscript; available in PMC 2014 July 09.

Published in final edited form as:

Nature. 2014 January 9; 505(7482): 223–228. doi:10.1038/nature12808.

TRANSCRANIAL AMELIORATION OF INFLAMMATION AND CELL DEATH FOLLOWING BRAIN INJURY

Theodore L. Roth, **Debasis Nayak**, **Tatjana Atanasijevic**, **Alan P. Koretsky**, **Lawrence L. Latour**, and **Dorian B. McGavern**

National Institute of Neurological Disorders and Stroke, National Institutes of Health, Bethesda, MD 20892

Abstract

Traumatic brain injury (TBI) is increasingly appreciated to be highly prevalent and deleterious to neurological function [1, 2]. At present no effective treatment options are available, and little is known about the complex cellular response to TBI during its acute phase. To gain novel insights into TBI pathogenesis, we developed a novel closed-skull brain injury model that mirrors some pathological features associated with mild TBI in humans and used long-term intravital microscopy to study the dynamics of the injury response from its inception. Here we demonstrate that acute brain injury induces vascular damage, meningeal cell death, and the generation of reactive oxygen species (ROS) that ultimately breach the glial limitans and promote spread of the injury into the parenchyma. In response, the brain elicits a neuroprotective, purinergic receptor dependent inflammatory response characterized by meningeal neutrophil swarming and microglial reconstitution of the damaged glial limitans. We additionally show that the skull bone is permeable to small molecular weight compounds and use this delivery route to modulate inflammation and therapeutically ameliorate brain injury through transcranial administration of the ROS scavenger, glutathione. Our results provide novel insights into the acute cellular response to TBI and a means to locally deliver therapeutic compounds to the site of injury.

TBI encompasses injuries that range from mild to severe [1, 3] and occurs when the brain is exposed to external forces that induce focal and / or diffuse pathologies, including vascular damage, edema, axonal shearing, and neuronal cell death [4–6]. TBI is usually divided into two phases: the primary insult and ensuing secondary reaction. It is postulated that primary cell death cannot be prevented without avoiding the injury itself, but that secondary damage is amenable therapeutic intervention because it is driven by pathogenic parameters such as ROS [7, 8], calcium release [9], glutamate toxicity [10, 11], mitochondrial dysfunction [12], inflammation [6], *etc*. To date, animal models of TBI have been developed that reflect mild,

Corresponding author: Dorian B. McGavern, Ph.D., NIH / NINDS, 10 Center Drive, Bethesda, MD 20892, Phone: (301) 443-7949, mcgavernd@mail.nih.gov.

CONTRIBUTIONS

T.L.R., D.N., and D.B.M. designed all murine experiments and interpreted the data. L.L.L. provided and interpreted the human TBI data. T.A. and A.P.K. contributed the transcranial manganese data. T.L.R. and D.B.M. wrote the paper.

COMPETING FINANCIAL INTERESTS

The authors declare no competing financial interests.

moderate, and severe forms of injury [5], but therapeutic research in these models has not yet translated successfully into the clinic [4, 13]. Thus, there is an increasing need to develop additional TBI models, temporally map the dynamics of brain injury responses, and devise therapeutic interventions.

In humans, primary injury to the meninges and vasculature can be observed in the absence of conspicuous brain damage following minor head trauma. As part of an ongoing study of mild TBI, we evaluated research MRI with contrast from patients presenting to the emergency room within 48 hours of minor head injury. Over a period of 30 months, 142 patients were enrolled with a baseline Glasgow Coma Scale (GCS) of 15, reporting loss-of-consciousness or post-traumatic amnesia, and a clinical computed tomography (CT) scan without evidence of injury to the parenchyma. Meningeal hemorrhage was seen on CT in 18 patients (12.7%), including subarachnoid blood in 13 (9.1%) and subdural blood in 7 (4.9%). Focal enhancement of the meninges was observed on post-contrast FLAIR MRI imaging (Fig. 1a) in 69 (48.6%) patients, and without concomitant meningeal hemorrhage in 53 (36.9%) patients. Enhancement is the result of extravasation of gadolinium contrast into space containing free fluid with a T1 relaxation time constant equivalent to that of cerebrospinal fluid (CSF) [14].

To better understand the immunopathogenesis of focal brain injury, we developed a novel closed-skull model of mild TBI amenable to intravital imaging studies. Thinning the murine skull bone to ~30 μm allows the underlying meninges and brain parenchyma to be imaged by two-photon laser scanning microscopy (TPM) without overt brain injury or inflammation [15]. Thinning the skull bone beyond 30 μm causes increased pliability and concavity, which compresses the meningeal space (referred to as a compression injury) (Extended Data Fig. 1). Sequential thinning of the skull bone from 50 to 10 μm induced increasing amounts of meningeal cell death (Fig. 1b). Cell death and inflammation associated with over-thinning was reproducibly generated by quickly thinning the skull bone to ~20–30 μm and then manually promoting concavity with minimal downward pressure (Extended Data Fig. 1). We used this model to define the dynamics of inflammation and mechanisms that cause cell death following focal TBI.

Using TPM we first mapped the kinetics and severity of brain pathology starting 5 min following compression injury. Immediately after injury quantum dots injected intravenously leaked from vessels into the subarachnoid and perivascular spaces (Fig. 1c; Video 1). Within 30 minutes, ROS was detected in the meninges (Fig 1d) and holes appeared in the glial limitans due to astrocyte cell death (Fig. 1e; Video 1). Transcranially administered SR101 leaked through the glial limitans into the parenchyma after compression injury, but remained largely within the meningeal space following standard skull thinning (Fig. 1f). Compression also induced cell death in the meninges that increased steadily over time, but was not observed in the parenchyma until 9–12 hrs post-injury (Fig. 1g, h). Parenchymal cell death at 12 hrs was indiscriminate, as neurons, astrocytes, oligodendrocytes, and microglia were all lost in the lesion site (Extended Data Fig. 2).

We next sought insights into the dynamics of the innate inflammatory response. Meningeal macrophages (long, rod-like cells) died within 30 min of compression injury (Fig. 2a; Video

1). In response to meningeal cell death, microglia extended processes through the compromised glial limitans into the meninges (Extended Data Fig. 3a; Video 1). We also observed a coordinated microglial response to compression injury. Most microglia within 50 μm of the meninges retracted all processes except for ~2–3 that extended towards the glial limitans, forming a stable contiguous network resembling a “honeycomb” structure (Fig. 2b; Video 2). Long-term TPM revealed that the honeycomb network formed within an hour of injury and could be maintained for up to 12 hrs (Video 2). Honeycomb microglia surrounded surviving astrocytes in the glial limitans and aligned with the junctions between individual cells (Extended Data Fig. 3b; Video 2).

In response to astrocyte death (Fig. 1d; Video 1), a morphologically distinct microglial reaction was observed; microglia retracted their ramified processes and extended a single, non-branching process towards the glial limitans that resembled a “jellyfish” (Fig. 2c; Extended Data Fig. 3b; Video 3). Jellyfish microglia started to form almost immediately after compression injury (Videos 3,4), and some were motile, whereas others remained stationary (Videos 3–5). We commonly observed honeycomb networks of microglia interspersed with clusters of jellyfish microglia (Videos 4,5), which likely reflects variation in lesion severity along the glial limitans. Honeycomb microglia could even transform within 5 min into jellyfish, presumably following astrocyte cell death (Video 5), whereas naïve microglia required ~30 min to acquire a jellyfish morphology. Jellyfish projections were usually linked to cell bodies via thin processes (Video 5) and often formed a continuous phagocytic layer at the glial limitans (Fig. 2c; Extended Data 3b; Videos 3, 6, 7). Over time, microglia residing in the glial limitans died, particularly after tissue swelling (or edema) was observed (Video 7). Peripherally-derived myelomonocytic cells (neutrophils and monocytes) also responded to brain damage. Within an hour of compression injury, myelomonocytic cells (likely neutrophils) localized exclusively to the meninges, were highly motile, and interacted with dead cells during the 12 hr observation period (Fig. 2d; Video 8).

To modulate TBI lesions locally, we applied compounds to the intact skull bone. We discovered that SR101, a 600 molecular weight (MW) dye, when applied to an intact (non-thinned) skull bone passed directly into the meninges within 10 min (referred to as a “transcranial application”) (Fig. 3a). We next tested a range of different sized fluorescent dextrans (3K to 70K MW). Dextrans of 40K MW and below were able to pass through the intact skull into the meninges (Fig. 3b), although larger dextrans required longer diffusion times (Fig. 3c). A 70K MW dextran was unable to pass transcranially in 30 min. In addition, a variety of fluorescent small molecules and macromolecules passed through the murine skull bone and achieved measurable steady state concentrations in the meninges dependent on molecular weight (Fig. 3d, Extended Data Fig. 4). Passage through an intact skull yielded a meningeal concentration approximately one half of that achieved by thinned skull application (Extended Data Fig. 4d, e). We assessed the feasibility of passing compounds through thicker skulls by applying the contrast agent manganese chloride to an intact rat skull bone (~1 mm thick) and imaging transcranial passage by MRI (Fig. 3e). Transcranially applied manganese chloride was clearly visible in the rat brain parenchyma 2 hrs after application.

We next defined the mechanisms underlying compression injury induced inflammation. Trancranial application of purinergic receptor [16] (P2Y12 or P2X4) inhibitors prior to compression injury prevented both honeycomb and jellyfish morphologies, whereas P2Y6 antagonism only blocked the jellyfish response (Fig. 4a,b; Extended Data Fig. 5a; Video 9). In contrast, P2X7 antagonism had no effect on microglia, but almost entirely eliminated neutrophil recruitment (Fig. 4a–c; Extended Data Fig. 5b; Video 9). Astrocytes are known to amplify purinergic receptor signaling through ATP-induced ATP release via connexin hemichannels, which can be blocked with carbenoxolone (CBX) [17]. Transcranial application of CBX, but not a specific pannexin inhibitor (probenecid), prior to compression injury caused microglia to remain ramified, extending only small, ill-defined circular processes at the glial limitans similar to P2Y6 antagonism (Fig. 4d,e; Extended Data Fig. 5c; Video 9). CBX inhibited the formation of honeycomb and jellyfish microglia, whereas pannexin inhibition slowed the onset and magnitude of neutrophil recruitment (Fig. 4f). Pre-treatment with CBX also significantly increased SR101 leakage through the glial limitans, suggesting that ATP release by astrocytes and purinergic signaling in microglia help maintain barrier integrity between the meninges and parenchyma (Fig. 4g; Extended Data 5d).

To identify the primary mediator of cell death following compression injury, we focused on the role of ROS, which appeared in the meninges shortly after compression injury (Fig. 1d). Transcranial administration of the ROS scavenger, glutathione (GSH), resulted in near complete survival of meningeal macrophages following a more severe injury (i.e., skull fracture) (Fig. 5a; Video 10) as well as glial limitans preservation (Fig. 5b, f). In addition, microglia beneath this layer remained in a non-reactive, ramified state (Fig. 5a, e; Video 10). Preservation of the glial limitans following GSH treatment resulted in refilling of the subarachnoid space beneath the compression injury, which pushed the thinned skull bone upward (Video 10). GSH administration also eliminated the recruitment of myelomonocytic cells (Fig. 5c, g; Video 10).

Cell death was first observed in the meninges and later spread to the parenchyma following compression injury (Fig. 1h). Transcranial pretreatment with GSH resulted in a 50% reduction in meningeal death, but administration after injury had no effect (Fig. 5h), indicating that half the initial meningeal cell death following compression injury is due to ROS. GSH when applied continuously starting at 15 min or 3 hrs post-injury reduced parenchymal cell death at 12 hrs by 67% and 51%, respectively (Fig. 5d, i). These data indicate that ROS is a mediator of cell death following compression injury. The contribution of inflammation to cell death was assessed by transcranially inhibiting neutrophils and microglia with P2X7 or P2Y6 antagonism, respectively. Inhibition of neutrophil recruitment through P2X7 antagonism increased cell death in the meninges 12 hrs later, but had no impact on parenchymal cell death (Fig. 5h, i). Conversely, inhibition of microglia through P2Y6 antagonism increased parenchymal cell death at 12 hrs, but had no impact on meningeal cell death (Fig. 5h, i). These data suggest that inflammation is neuroprotective within the first 12 hrs of compression injury.

TBI induces a complex reaction that can result in permanent damage and neurological dysfunction. In this study, we observed evidence of meningeal damage in ~50% of patients with mild head injury, indicating that this is a common pathology in humans. We sought

mechanistic insights into this process by developing a novel closed-skull model of brain injury and imaging the acute cellular injury response from its inception. Importantly, we discovered that the skull bone is porous and permits the passage of small molecules (≤ 40K MW) and contrast agents by passive diffusion, which should facilitate local delivery of therapeutics and other molecules into the CNS. Pathologically, compression injury initially caused meningeal cell death, vascular damage, ROS generation, and disruption of the glial limitans, which ultimately gave rise to indiscriminate parenchymal cell death. ROS is commonly observed in TBI lesions [7, 8], and transcranial delivery of GSH preserved the glial limitans, reduced cell death, and eliminated the sterile injury response. GSH significantly reduced parenchymal cell death even when administered 3 hrs after injury, providing a therapeutic window for treatment of focal brain injury.

In the absence of GSH, the brain responded to damage by eliciting an anatomically partitioned sterile immune reaction [18]. Microglia first fortified the glial limitans through the generation of honeycomb and jellyfish structures. Honeycomb microglial networks circumscribed individual surviving astrocytes in the glial limitans and were induced to do so by release of ATP from connexin hemichannels and detection by purinergic receptors (P2X4 and P2Y12) [16, 17, 19, 20]. Phagocytic jellyfish microglia were similarly generated by purinergic signaling (P2X4, P2Y6, P2Y12) and filled areas along the glial limitans in which astrocyte cell death had occurred. Transcranial inhibition of the microglial response through P2Y6 or connexin hemichannel antagonism increased glial limitans permeability and parenchymal cell death following compression injury. While microglia protected the parenchyma, myelomonocytic cells invaded the damaged meninges in a P2X7- and pannexin-dependent manner consistent with a recent study showing P2X7-dependent neutrophil recruitment into the injured liver [21]. Collectively, our data suggest that the acute inflammatory reaction to brain injury is beneficial [6]. Moreover, ROS and purines represent major drivers of the injury response and are amenable to transcranial therapeutic manipulation.

METHODS SECTION

Human Subjects and MRI protocol

As part of the ongoing Traumatic Head Injury Neuroimaging Classification (THINC) study, patients presenting to the emergency room or trauma service at Suburban Hospital (SH, Bethesda, MD) and MedStar Washington Hospital Center (WHC, Washington, DC) within 48 hours of head injury are screened and enrolled (NCT01132937). In most patients, a conventional non-contrast CT scan was obtained for clinical purposes. Following consent, a research MRI was obtained that included a single dose of a gadolinium based contrast agent: 0.1 mmol/kg gadopentetate dimeglumine (Bayer HealthCare) or 0.2 mmol/kg gadobenate dimeglumine (Braco Diagnositcs) according to local site policy. The imaging was performed on either a 1.5T (SH) or 3T (WHC) scanner using a protocol of ~25 minute duration, which included T2-FLAIR (fluid attenuated inversion recovery) of ~2:30 duration, obtained before and again 5 min after intravenous (i.v.) contrast administration. An additional 3D-T2-FLAIR sequence was acquired post-contrast on the 3T at WHC to permit better visualization of the

morphology of enhancement on a surface rendering of the head. This study was approved by the NINDS Institutional Review Board.

Rodents

C57BL/6J (B6), B6.129P-*Cx3cr1*^{tm1Litt}/J (CX3CR1$^{gfp/gfp}$) [1], and FVB/N-Tg(GFAPGFP)14Mes/J [2] mice were obtained from The Jackson Laboratories. CX3CR1$^{gfp/+}$ mice were generated by crossing B6 mice with CX3CR1$^{gfp/gfp}$ mice in a closed breeding facility at the National Institutes of Health (NIH). B6 LysM-GFP heterozygous knock-in mice (LysM$^{gfp/+}$) were generously provided by Dr. Thomas Graf (Albert Einstein College of Medicine) [3] and maintained at the NIH. All mice were 8–16 weeks of age. Adult male Sprague-Dawley rats (body weight ~ 200 g) were obtained from Harlan Laboratories. All rodents were housed under specific pathogen-free conditions and treated in accordance with Institutional Animal Care and Use Committee at the NIH.

Skull Thinning & Compression Injury

For imaging experiments, mice were anesthetized with ketamine (85 mg/kg), xylazine (13 mg/kg), and acepromazine (2 mg/kg) in PBS and maintained at a core temperature of 37°C. The skull bone over the barrel cortex was then thinned to a thickness of ~30–40 μm as described [4]. For this procedure, the bone was manually thinned over a 30 minute period, and the amount of downward pressure was kept to a minimum. To induce a compression injury, the skull was thinned within 1–2 min to a thickness of ~20–30 μm. Once thinned, the blunt end of a surgical instrument was used to gently press the pliable skull bone downward to promote concavity in the bone. The downward pressure applied was minimal and only performed until a concave bone was observed. This resulted in the skull bone collapsing (without breaking) inward toward the surface of the brain. In one set of experiments, the skull bone was intentionally cracked to induce a severe injury. Imaging was performed beginning 5 min after injury.

Intravital two-photon laser scanning microscopy

Mice with a normally thinned or compressed skull bone were imaged using a Leica SP5 two-photon imaging system (Leica Microsystems, Bannockburn, IL) equipped with an 8000 Hz resonant scanner, a 20× / 1.0 NA dipping objective, and two Mai Tai HP DeepSee Lasers (SpectraPhysics) tuned to 905, 920 or 970 nm. Fluorescence emission was separated by high efficiency custom dichroic mirrors (Semrock) and collected with a NDD4 external detector (Leica). Stacks of images were acquired using a step size of 1.0 μm (single stacks) or 2.5 μm (time lapse videos) to a depth of 150 μm. Time lapse videos were acquired with 1 min intervals between 3D stacks. For all imaging studies, the 20× lens was submerged directly into artificial cerebral spinal fluid (aCSF; 119 mM NaCl, 26.2 mM $NaHCO_3$, 2.5 mm KCl, 1 mM NaH_2PO_4, 1.3 mM $MgCl_2$, 1.2 mM $CaCl_2$, 0.4 % glucose, pH 7.4) placed atop the thinned skull.

Fluorescent dyes

To visualize brain vasculature, mice were injected i.v. 10 min prior to imaging with 50 μl Qtracker 655nm non-targeted quantum dots in PBS (0.2 μM; Invitrogen). Cell death was

visualized by incubating the thinned skull with propidium iodide (1.5 mM) in aCSF for 30 min. This was followed by a single wash with aCSF and then imaging. Reactive oxygen species (ROS) were visualized by applying Amplex Red (500 μM) transcranially for 10 min. This was followed by immediate imaging. Astrocytes were visualized by transcranially applying SR101 (10 mM) for 30 min. This was followed by a 1 hr aCSF wash and then imaging.

Immunohistochemistry

To examine the identity of dead cells in the brain parenchyma, a compression injury and normal thin skull procedure were performed on opposite hemispheres of the same skull. Dead cells were labeled by transcranial propidium iodide application, and the mice were perfused with 4% paraformaldehyde (PFA) at 12 hours post injury. Whole mouse heads were post-fixed in 4% PFA for 8 hrs and then stored in 30% sucrose for another 24 hrs. After decalcification of the skull bone, 6-μm serial coronal brain sections through the injury and control sites were produced by Histoserv, Inc. (Germantown, MD). Prior to antibody staining, sections were blocked with 10% fetal bovine serum (FBS) (GFAP and Iba1 stains), 10% FBS + 35 μg/ml donkey anti-mouse F(ab) (NeuN stain), or 10% FBS + 35 μg/ml donkey anti-mouse F(ab) + 0.1% Triton X100 (APC stain). The following cell types were labeled: neurons (anti-NeuN; 1:800; Chemicon), astrocytes (anti-GFAP; 1:800; DakoCytomation), microglia (anti-Iba1; 1:400; Wako), and oligodendrocytes (anti-APC; 1:50; Oncogene Research). Cell marker-specific antibodies were detected with secondary antibodies conjugated to Alexa Fluor 488 (1:200; Jackson ImmunoResearch Laboratories). Working stocks of primary and secondary reagents were diluted in PBS containing 2% FBS (NeuN, GFAP, IbaI) or 10% FBS with 0.1% Triton X100 (APC). All sections were incubated with 1 μg/mL 4,6-diamidino-2-phenylindole (DAPI; Sigma-Alderich) for 3 min at room temperature to stain cell nuclei.

Confocal Microscopy

2D images shown in Figure S2 were captured from stained 6-μm frozen sections using an Olympus FV1200 confocal microscope equipped with 20× objective. Images were collected using sequential scanning with the 405, 488, and 559 nm laser lines to produce three color overlays.

Purinergic receptor, hemichannel, and ROS antagonism

Prior to skull thinning, antagonists diluted in aCSF were applied directly to the skull bone, and vehicle was simultaneously applied to the opposite hemisphere to serve as a control. The following antagonists from Sigma were used: TNP-ATP hydrase (P2X4; 25 mM), oxidated ATP (P2X7; 10 mM), MRS2578 (P2Y6; diluted a 50 mM DMSO stock 1:100 in aCSF to a final concentration of 500 μM), MeSAMP (P2Y12; 10 mM), carbenoxolone (CBX) (connexin hemichannels; 100 mM), Provenecid (pannexin hemichannels; 100 mM), and glutathione (ROS; 100 mM). Vehicle and purinergic receptor antagonists were applied as a 3 mm diameter bubble on the skull surface and replenished as needed over a 30 min incubation period to prevent drying. This allowed the antagonists to continuously pass through the skull bone. Following the 30 min incubation, the skull was dried and then thinned to induce a compression injury over both hemispheres. Imaging was initiated

immediately after injury. For most studies, the skull bone pre-incubated with antagonists was imaged continuously for 3–10 hrs, after which a 3D stack was captured from both the vehicle and antagonist treated areas for quantitative purposes. Long term continuous intravital TPM alone did not induce an injury response (**data not shown**). Glutathione was also applied at 15 min and 3 hrs following compression injury to determine the impact on cell death. For these studies, glutathione was added directly to the aCSF submerging solution (100 mM) while imaging. The glutathione was maintained in the submerging solution for the entire imaging experiment. Similar studies were conducted using 10 mM oxidated ATP and 500 μM MRS2578.

Glial limitans leakage assay

For permeability studies, areas of skull bone were pre-incubated with vehicle, CBX (100 mM), or glutathione (100 mM) for 30 min as described above. Afterward, a meningeal compression injury was induced. While imaging, antagonists (10 mM CBX or 100mM glutathione) were added directly to the aCSF submerging solution. After 3 hrs of imaging, SR101 (1 mM) was applied for 15 minutes, followed by a 5 min aCSF wash. A 3D stack was then captured to quantify the degree of SR101 leakage through the glial limitans.

Skull bone permeability analyses

For skull bone permeability studies, the following rhodamine-labeled dextrans were placed directly on the intact skull bone for up to 30 min: 3,000 MW (25 mM), 10,000 MW (5 mM), 40,000 MW (1 mM), and 70,000 MW (0.5 mM). SR101 (1 mM) was used as a representative of 600 MW compound. Compounds were replenished as needed to prevent drying. Following the incubation period, the skull bone was quickly thinned and imaged. A 3D stack was captured to determine if the fluorescence could be found beneath the skull bone. For quantitative analyses of skull bone permeability through a thinned skull window, the following fluorescent compounds were used: Nile Red (318 MW; 100 nM), fluorescein (376 MW; 100 nM), SR101 (606 MW; 100 nM), rhodamine DHPE (phospholipid; 1334 MW; 1 mM), 5-TMR-RRADDSDDDDD (TMR tagged peptide; 1706 MW; 100 nM), 5’-/ RhoR-XN/ ATGAT-3’ (Rhodamine Red tagged oligonucleotide; 2335 MW; 1 μM), 3,000 MW Dextran (100 nM), 10,000 MW Dextran (10 μM), and 40,000 MW Dextran (25 μM). Briefly, a thin skull preparation as described above was performed on a B6 mouse followed by 30 min of imaging in aCSF to establish a baseline. Without interrupting the imaging sequence, the aCSF was replaced after 30 min with a solution containing the fluorescent compounds at the denoted concentrations and then imaged continually for another 60 min. Following acquisition, 100 × 100 × 5 μm (xyz) boxes were created using the ‘surfaces’ tool in Imaris and placed 25 μm above the skull, in the meninges (0–5 μm below the skull), and in the parenchyma (15–20 μm below the skull). The background fluorescence intensity for each anatomical region was calculated using the first 30 min of imaging. Instantaneous concentrations of fluorescent compounds were then determined from 30 to 90 min (at 1 min intervals) for the skull, meninges, and parenchyma by calculating the average fluorescent intensities in the 100 × 100 × 5 μm boxes. After subtracting the background fluorescence, the resultant number was divided by the fluorescent intensity of the applied compound in solution and multiplied by 100 to generate a percentage. To determine the concentrations in the meninges achieved by transcranial loading through an intact murine skull bone, 100 nM

SR101 was applied transcranially through the intact skull for 20 min followed by a quick (~2 min) thin skull preparation and imaging. The background fluorescence in the meninges and fluorescence intensity of 100 nM SR101 in aCSF were determined in a separate mouse as described above.

Transcranial manganese delivery

Rats were anesthetized with 5% isoflurane and then switched to 1–2% isoflurane for maintenance. Their body temperature was maintained by a heated water bath. The animals were placed in a stereotaxic apparatus, a single midline incision with a sterile scalpel was made through the skin of the skull, and the skull bone was exposed by scraping away the periosteum. The following sterile saline solutions were placed directly on the skull bone above S_1 area (left/right: +3, rostral/caudal: −1.4, from Bregma): 500mM $MnCl_2$, 250mM $MnCl_2$ (not shown), and pure saline as a control. The solutions were pipetted over a 2 hr period and replenished as needed. After 2 hrs, the skull was rinsed three times with saline, the skin sutured, and the animal promptly placed in a MRI scanner to detect manganese diffusion into the brain. Images were acquired on an 11.7 T/31 cm horizontal magnet (Agilent, Oxford, UK) interfaced to a Bruker Avance III console (Bruker BioSpin, Billerica, MA) equipped with a 12-cm gradient set (Resonance Research Inc., Billerica, MA). A 9-cm laboratory-built birdcage coil was used for signal transmission and a 2-cm surface coil placed on the rat head was used for signal acquisition. During imaging, anesthesia was maintained at 1.5% isoflurane, and the body temperature was maintained at 37°C via a heated water bath. Contrast enhancement by manganese was detected using a T_1-weighted spin echo pulse sequence (TE=7.6 ms, TR=500 ms, Nav=8, 100 μm in-plane resolution, thirty 1-mm thick axial slices). The T_1 relaxation times were measured using a saturation recovery spin-echo sequence (TE=7.6 ms, TRs=0.4; 0.97; 1.77; 3.124 and 10s, 200 μm in-plane resolution).

Two-photon image analysis

All quantitative analyses and processing of 3D / 4D imaging data were performed using Imaris 7.0 software (Bitplane). Supplemental videos were constructed and annotated using Adobe Premiere Pro CS4. Microglia “honeycomb” reactions were quantified from 434 × 434 × 150 μm (xyz) 3D image stacks obtained at selected time points in $CX3CR1^{gfp/+}$ mice. This was accomplished by measuring the total length of microglial processes in contact with the glial limitans. Microglial cell bodies were first selected using the Imaris “spots” tool. Afterward, 10 microglia per mouse were randomly selected for quantification of process length. Only cells with all of their processes in the field of view and no more than 50 μm beneath the skull bone were quantified. Microglial processes that were touching (flat against) the glia limitans were labeled and measured using the Imaris “filaments” tool. Data were then represented on a per cell basis as the length of microglial processes in contact with the glial limitans. Microglia with a “jellyfish” morphology were identified as those having processes greater than 20 μm in diameter. The number of “jellyfish” microglia was then divided by the total number of microglia within 50 μm of the skull bone and multiplied by 100 to generate a percentage. To quantify cell death, propidium iodide-positive cells were labeled in 3D stacks using the Imaris “spots” tool. Dead cells from 0 to 5 μm below the compressed skull were considered meningeal, whereas cells from 5 to 100 μm were

considered parenchymal. The number of dead cells was divided by the volume analyzed and represented as cells per mm^3. Neutrophils were quantified in $LysM^{GFP/+}$ mice using the Imaris "spots" tool. Following compression injury, neutrophils were never observed in the brain parenchyma, and, therefore, were quantified only in the meningeal space (0 to 5 μm below the compressed skull). The number of neutrophils was divided by the volume analyzed and represented as cells per mm^3. To quantify leakage of SR101 through the glial limitans, a 50 × 50 × 100 μm (*xyz*) solid box was generated using the Imaris "surfaces" tool. The box was placed 25 μm beneath the epicenter of the compression injury (i.e. the lowest point of the compressed skull bone). The mean fluorescent intensity of SR101 signal inside of this box was then calculated. The value obtained beneath the antagonist treated skull (glutathione or CBX) was divided by the vehicle control area (from the opposite hemisphere) to generate a fluorescence ratio.

MRI image analysis

MRI images from rats receiving transcranial Mn were analyzed using ImageJ (http://rsb.info.nih.gov/ij/) and MIPAV (http://mipav.cit.nih.gov/) software developed at NIH. T_1 relaxation maps for brain slices were calculated using the MRI Analysis Calculator plugin. Background tissue T_1 values and standard deviations for every slice were obtained by placing a region of interest (ROI) over an area of the cortex opposite from the one of manganese administration. T_1 relaxation maps were thresholded using the value of the background T_1 minus two standard deviations in order to obtain ROIs in which manganese had significantly shortened T_1 of the cortex tissue. The average T_1 relaxation times as well as total number of voxels in those ROIs were used to determine the local concentration and total amount of manganese in each slice, using the equation: $1 / (T_1)_{obs} = 1 / (T_1)_{backgr} + r_1 * c$. The value of 4.7 s^{-1} mM^{-1} was used for cortex T_1 relaxivity as previously reported [5]. The total amount of manganese was integrated through the relevant slices.

Group Sizes and Statistical Analysis

Group sizes of 3–4 rodents were used for all experiments to ensure reproducibility and that statistical differences could be detected. All experiments were independently replicated at least three times. Only animals that succumbed to anesthesia were excluded from further analysis. For experiments with experimental and control groups, littermates were randomized before assignment to a particular condition. Statistical significance ($p < 0.05$) was determined using a Student's *t* test (two groups) or a one way ANOVA (more than two groups). A Rank Sum test or ANOVA on ranks was used for datasets with non-parametric data. All graphs and statistical analyses were performed using SigmaPlot version 11.

Supplementary Material

Refer to Web version on PubMed Central for supplementary material.

ACKNOWLEDGMENTS

The study was supported by the National Institutes of Health (NIH), the National Institute of Neurological Disorders and Stroke (NINDS), and the Center for Neuroscience and Regenerative Medicine (CNRM) at the Uniformed Services University of the Health Sciences - a collaborative effort among NIH, the Department of

Defense, and Walter Reed National Military Medical Center to develop innovative approaches for brain injury diagnosis and recovery.

REFERENCES

1. Dekosky ST, Blennow K, Ikonomovic MD, Gandy S. Acute and chronic traumatic encephalopathies: pathogenesis and biomarkers. Nat Rev Neurol. 2013; 9:192–200. [PubMed: 23558985]
2. Roozenbeek B, Maas AI, Menon DK. Changing patterns in the epidemiology of traumatic brain injury. Nat Rev Neurol. 2013; 9:231–236. [PubMed: 23443846]
3. Zetterberg H, Smith DH, Blennow K. Biomarkers of mild traumatic brain injury in cerebrospinal fluid and blood. Nat Rev Neurol. 2013; 9:201–210. [PubMed: 23399646]
4. McConeghy KW, Hatton J, Hughes L, Cook AM. A review of neuroprotection pharmacology and therapies in patients with acute traumatic brain injury. CNS Drugs. 2012; 26:613–636. [PubMed: 22668124]
5. Xiong Y, Mahmood A, Chopp M. Animal models of traumatic brain injury. Nat Rev Neurosci. 2013; 14:128–142. [PubMed: 23329160]
6. Finnie JW. Neuroinflammation: beneficial and detrimental effects after traumatic brain injury. Inflammopharmacology. 2013
7. Hall ED, Andrus PK, Yonkers PA. Brain hydroxyl radical generation in acute experimental head injury. J Neurochem. 1993; 60:588–594. [PubMed: 8380437]
8. Lewen A, Matz P, Chan PH. Free radical pathways in CNS injury. J Neurotrauma. 2000; 17:871–890. [PubMed: 11063054]
9. Young W. Role of calcium in central nervous system injuries. J Neurotrauma. 1992; 9(Suppl 1):S9–S25. [PubMed: 1588635]
10. Bullock R, et al. Evidence for prolonged release of excitatory amino acids in severe human head trauma. Relationship to clinical events. Ann N Y Acad Sci. 1995; 765:290–297. discussion 298. [PubMed: 7486616]
11. Bullock R, et al. Factors affecting excitatory amino acid release following severe human head injury. J Neurosurg. 1998; 89:507–518. [PubMed: 9761042]
12. Mazzeo AT, Beat A, Singh A, Bullock MR. The role of mitochondrial transition pore, and its modulation, in traumatic brain injury and delayed neurodegeneration after TBI. Exp Neurol. 2009; 218:363–370. [PubMed: 19481077]
13. Janowitz T, Menon DK. Exploring new routes for neuroprotective drug development in traumatic brain injury. Sci Transl Med. 2010; 2 27rv21.
14. Mamourian AC, Hoopes PJ, Lewis LD. Visualization of intravenously administered contrast material in the CSF on fluid-attenuated inversion-recovery MR images: an in vitro and animal-model investigation. AJNR Am J Neuroradiol. 2000; 21:105–111. [PubMed: 10669233]
15. Xu HT, Pan F, Yang G, Gan WB. Choice of cranial window type for in vivo imaging affects dendritic spine turnover in the cortex. Nat Neurosci. 2007; 10:549–551. [PubMed: 17417634]
16. Eltzschig HK, Sitkovsky MV, Robson SC. Purinergic signaling during inflammation. N Engl J Med. 2012; 367:2322–2333. [PubMed: 23234515]
17. Davalos D, et al. ATP mediates rapid microglial response to local brain injury in vivo. Nat Neurosci. 2005; 8:752–758. [PubMed: 15895084]
18. Chen GY, Nunez G. Sterile inflammation: sensing and reacting to damage. Nat Rev Immunol. 2010; 10:826–837. [PubMed: 21088683]
19. Nimmerjahn A, Kirchhoff F, Helmchen F. Resting microglial cells are highly dynamic surveillants of brain parenchyma in vivo. Science. 2005; 308:1314–1318. [PubMed: 15831717]
20. Haynes SE, et al. The P2Y12 receptor regulates microglial activation by extracellular nucleotides. Nat Neurosci. 2006; 9:1512–1519. [PubMed: 17115040]
21. McDonald B, et al. Intravascular danger signals guide neutrophils to sites of sterile inflammation. Science. 2010; 330:362–366. [PubMed: 20947763]

METHOD REFERENCES

1. Jung S, et al. Analysis of fractalkine receptor CX(3)CR1 function by targeted deletion and green fluorescent protein reporter gene insertion. Mol Cell Biol. 2000; 20:4106–4114. [PubMed: 10805752]
2. Zhuo L, et al. Live astrocytes visualized by green fluorescent protein in transgenic mice. Dev Biol. 1997; 187:36–42. [PubMed: 9224672]
3. Faust N, Varas F, Kelly LM, Heck S, Graf T. Insertion of enhanced green fluorescent protein into the lysozyme gene creates mice with green fluorescent granulocytes and macrophages. Blood. 2000; 96:719–726. [PubMed: 10887140]
4. Yang G, Pan F, Parkhurst CN, Grutzendler J, Gan WB. Thinned-skull cranial window technique for long-term imaging of the cortex in live mice. Nat Protoc. 2010; 5:201–208. [PubMed: 20134419]
5. Chuang KH, Koretsky AP, Sotak CH. Temporal changes in the T1 and T2 relaxation rates (DeltaR1 and DeltaR2) in the rat brain are consistent with the tissue-clearance rates of elemental manganese. Magn Reson Med. 2009; 61:1528–1532. [PubMed: 19353652]

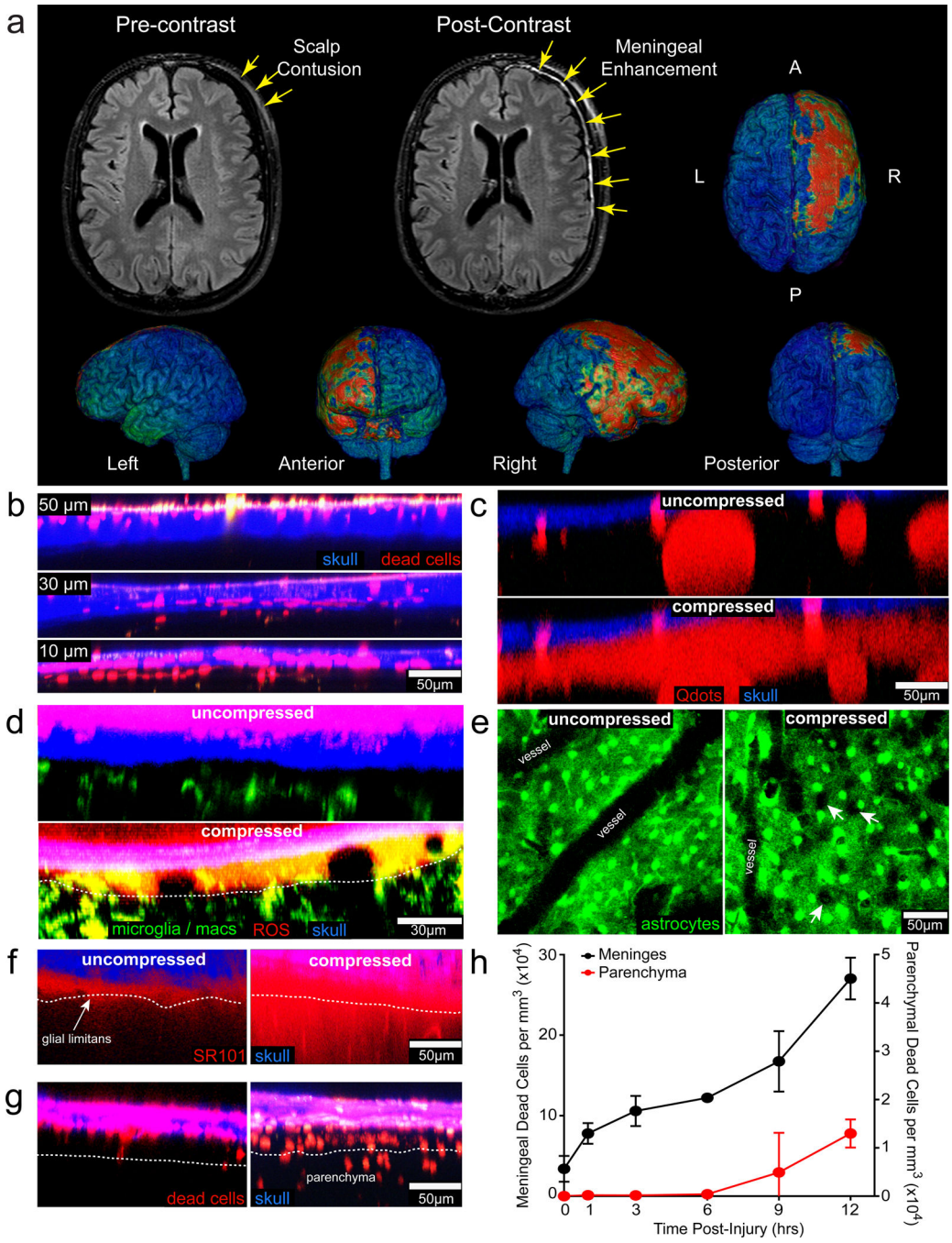

Figure 1. Pathology associated with compression injury

a, MRI of a patient's brain 19 hrs after fall from 6 feet, with reported loss-of-consciousness, post-traumatic amnesia, a Glasgow Coma Scale of 15 on arrival, and a negative CT scan. Following administration of Gd-DTPA contrast agent, FLAIR MRI (grayscale images) revealed focal enhancement in the meninges along convexity underlying the area of blunt trauma, better visualized on surface-rendered 3D-FLAIR (pseudo-colored 3D images) as involving the frontal and temporal lobes as well as anterior aspects of the cerebral falx. **b–d, f,g**, Maximum projections (5 µm wide) are shown in the *xz* plane of two-photon z-stacks

captured through a thinned skull. **b**, Images of skull bone (blue) and underlying meninges show sequential skull thinning from 50 to 10 μm. Dead cells (red) were labeled by transcranial propidium iodide (PI) administration. **c**, Intravenously injected Q-dots (red) leak from blood vessels into the meninges 15 min following compression injury, indicative of vascular damage. **d**, ROS (red) labeled with Amplex Red appears in the meninges 30 min following compression injury of CX3CR1$^{gfp/+}$ (green) mice relative to uncompressed controls. (white dotted line = glial limitans) **e**, *xy* maximal projections (25 μm in depth) captured in GFAP-GFP mice show holes (white arrows) in the glial limitans as a result of astrocyte (green) death, which starts to occur 5 min after compression injury. **f**, Transcranially applied SR101 (red) diffuses into the brain parenchyma 30 min after injury, but is largely excluded from the parenchyma in an uncompressed control mouse. **g**, Cell death (PI+ cells; red) becomes apparent in the brain parenchyma 12 hrs following compression injury and is not observed in uncompressed controls. **h**, Quantification of cell death (mean + SD) in the meninges and parenchyma following compression injury. All data in the figure are representative of 3 mice per group (4 mice, **g**) and at least three independent experiments.

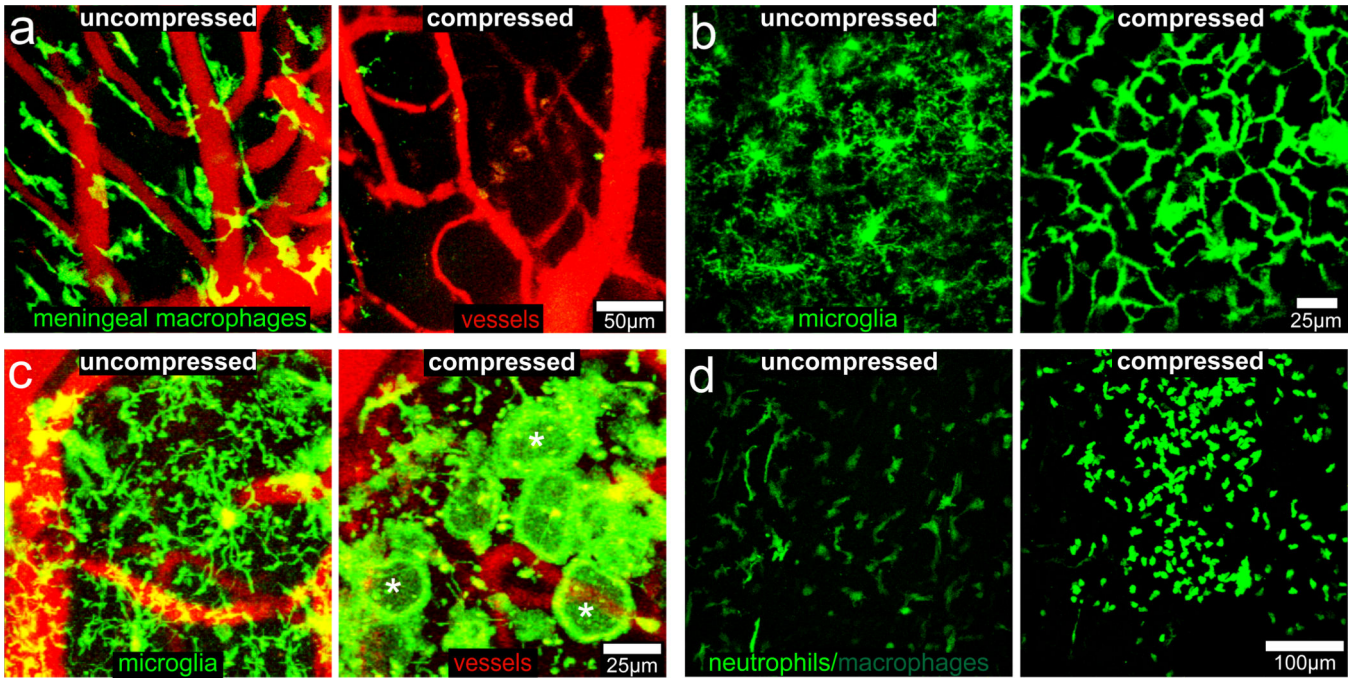

Figure 2. Innate immune response to a compression injury

25 μm *xy* maximum projections from CX3CR1$^{gfp/+}$ mice (**a–c**) or LysM$^{gfp/+}$ mice (**d**) captured at 30 min (**a**), 1 hr (**b**), 2 hrs (**c**), or 6 hrs (**d**) following a normal thinned skull preparation (uncompressed) or compression injury. **a**, Meningeal macrophages (green) visualized in CX3CR1$^{gfp/+}$ mice burst and die within 30 min of compression injury relative to uncompressed controls. Blood vessels are red. **b**, Microglia (green) retract their ramified processes and form a highly connected “honeycomb” network at the glial limitans following compression injury. **c**, A subset of microglia (green) after compression injury retract ramified processes and generate a single, flat, motile, phagocytotic process at base of glial limitans, resembling a “jellyfish” (examples denoted with white asterisks). Blood vessels are red. **d**, LysM$^{gfp/+}$ neutrophils (green) are recruited to the site of injury, but not to an uncompressed thinned skull window. Green cells residing in the uncompressed window represent meningeal macrophages. Data are representative of 3 mice per group and at least three independent experiments.

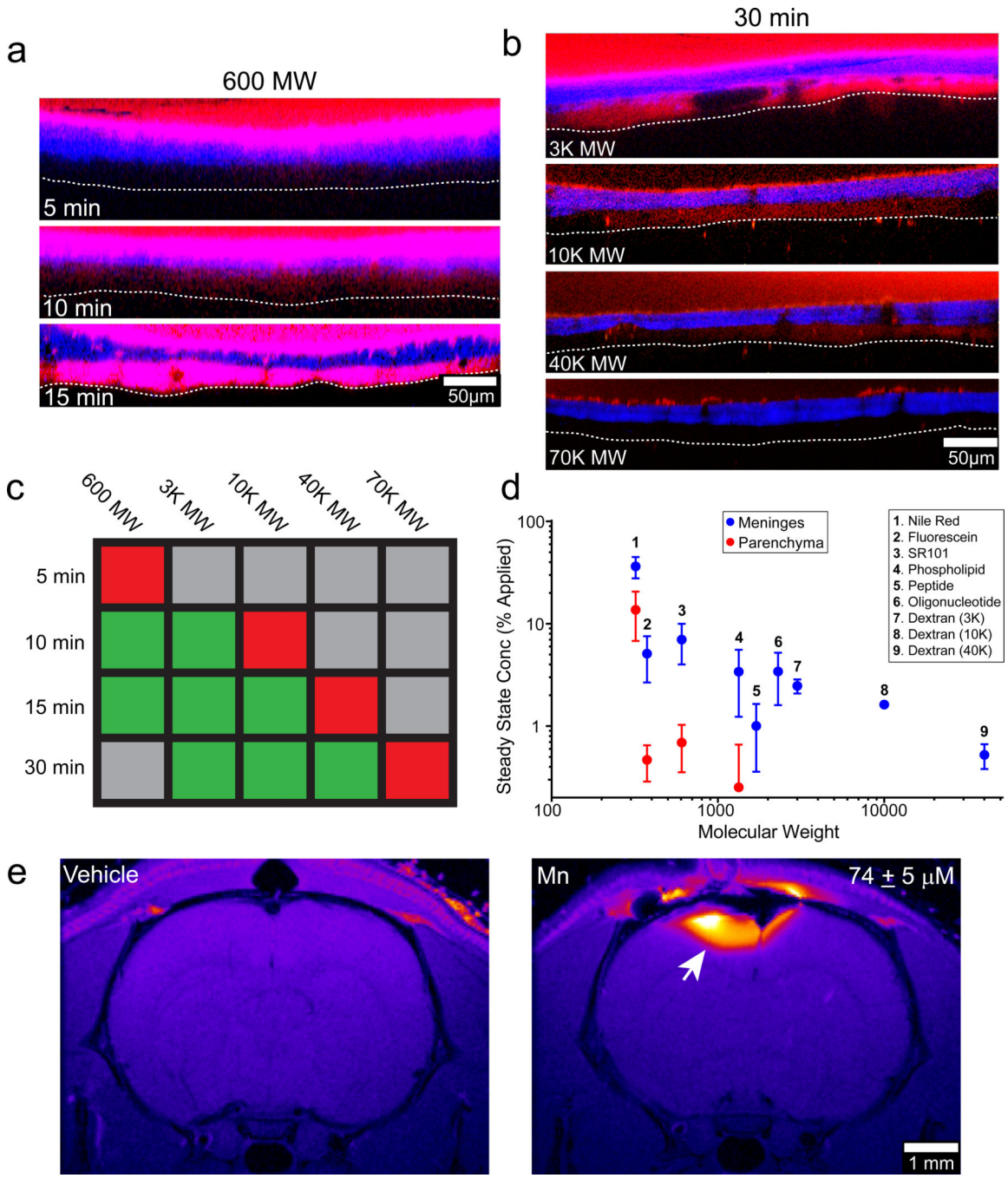

Figure 3. Metrics of transcranial diffusion through the skull bone

a, SR101 (red) was applied to an intact mouse skull for the indicated time and then the skull (blue) was quickly thinned and imaged. Five micron *xz* maximum projections show that SR101 is detectable in the meninges beginning 10 minutes after application and fully saturates the space within 15 min. (white dotted line = glial limitans) **b**, The size dependence of diffusion through an intact skull bone was evaluated 30 min following continuous transcranial application of the indicated MW dextrans (red). Dextrans that passed successfully through the skull generated fluorescence in the meninges. The skull bone is

shown in blue, and the glial limitans is denoted with a white dotted line. **c**, A color coded table summarizing the imaging results shown in panels **a** and **b** denotes the presence (green) or absence (red) of fluorescent dye in the meninges at the indicated MW and time. Gray = not tested. **d**, Fluorescent compounds of increasing molecular weights were passed transcranially through a thinned skull window during imaging. Steady state concentrations (mean + SD) of the fluorescent compounds in the meninges and parenchyma were quantified from normalized fluorescence intensities. See associated Figure S4. **e**, Manganese chloride (500 mM solution) applied transcranially to an intact rat skull (~1 mm thick) is visible by MRI in the brain parenchyma 2 hrs after application (white arrow). The mean parenchymal manganese concentration ± SD is provided. All data in the figure are representative of 3 mice (or rats) per group and at least three independent experiments.

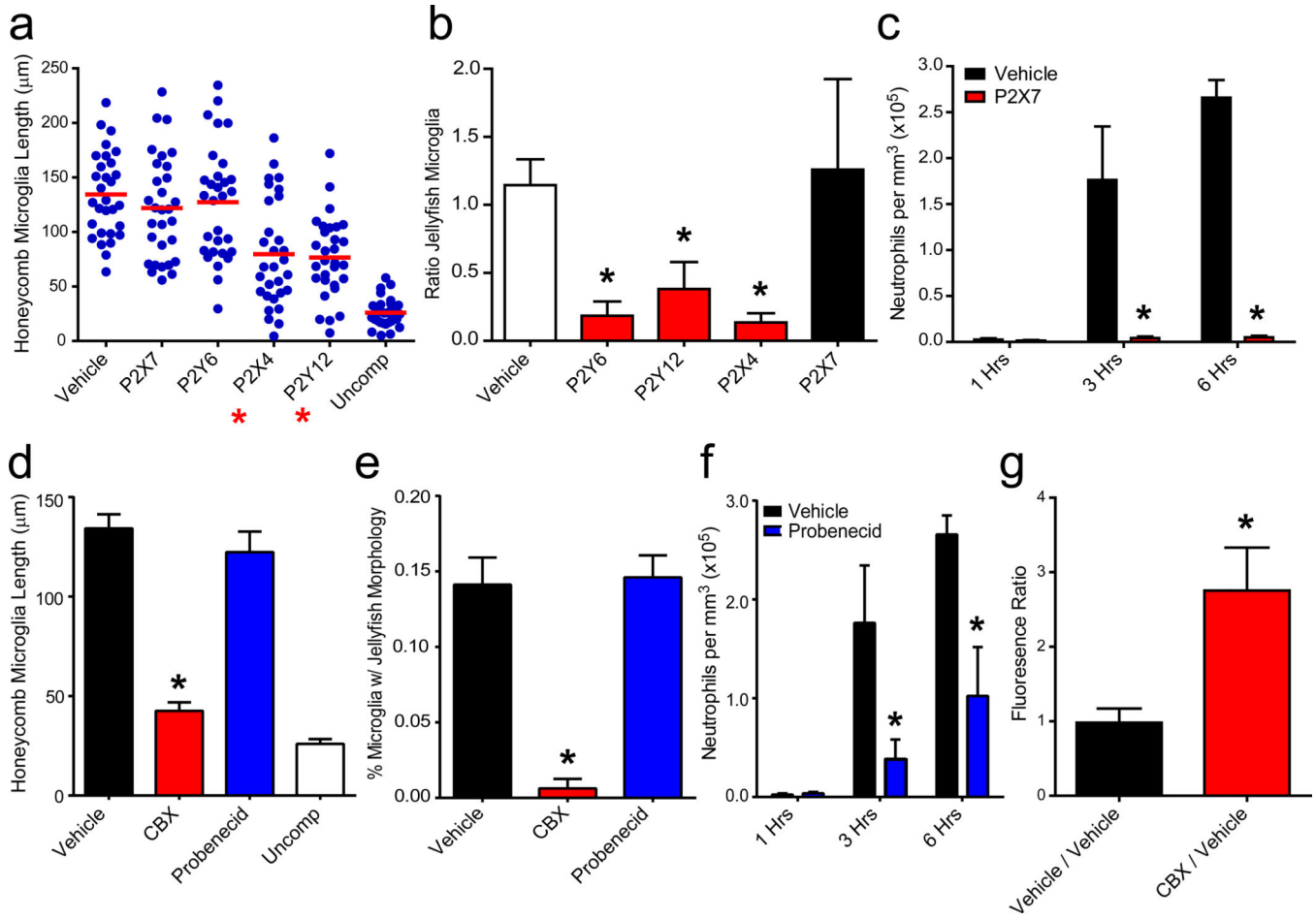

Figure 4. Purinergic receptor signaling mediates the innate immune response to compression injury

a, Honeycomb microglia were quantified 3 hrs following compression injury in mice treated transcranially with P2X7, P2Y6, P2X4, and P2Y12 antagonists or vehicle. Uncompressed mice served as a negative control. Blue dots represent individual microglia, and the horizontal red line denotes the mean. **b**, Quantification of jellyfish microglia was performed 3 hrs following compression injury. Because two compression injuries were generated per mouse, data are represented as a ratio (mean±SD) of purinergic receptor antagonist / vehicle and compared to vehicle / vehicle. A ratio of one signifies no difference between the two hemispheres. **c**, Quantification of neutrophils per mm^3 tissue (mean±SD) was performed at 1, 3, and 6 hrs post-compression injury. **d–f**, Bar graphs (mean±SD) show quantification of $CX3CR1^{gfp/+}$ microglia with a honeycomb (**d**) or jellyfish (**e**) morphology as well as the number $LysM^{gfp/+}$ neutrophils (**f**) following transcranial administration of CBX or probenecid. **f**, Glial limitans permeability was quantified by generating two compression injuries per mouse. The mean SR101 fluorescence in the parenchyma beneath each injury was calculated and expressed as a ratio (CBX / vehicle or vehicle / vehicle). A ratio larger than one signifies increased permeability in the experimental group. Asterisks in all figures denote statistical significance ($p < 0.05$) relative to the vehicle control group. Data are representative of 3 mice per group and at least three independent experiments.

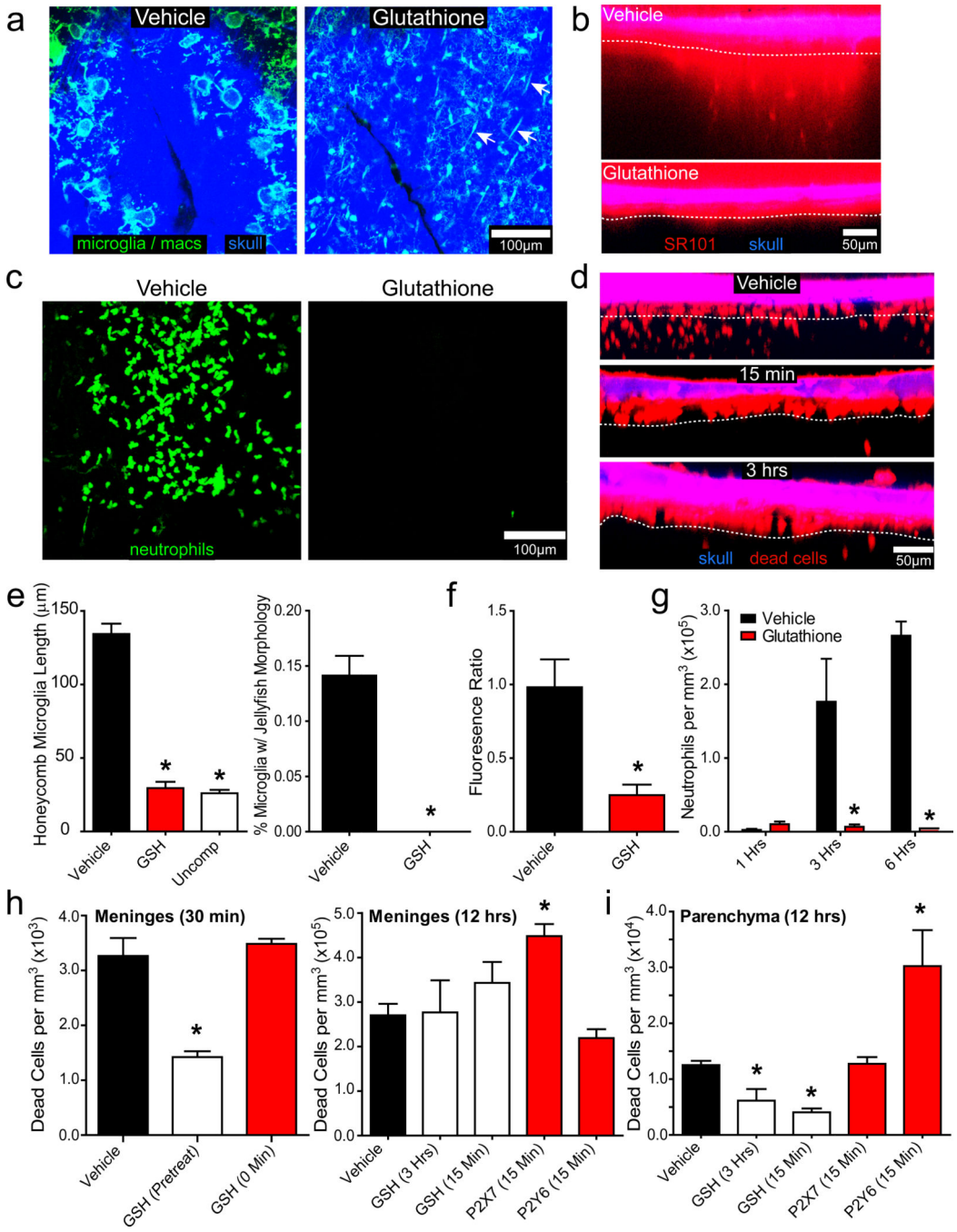

Figure 5. Transcranial administration of glutathione reduces inflammation and cell death following compression injury

25 μm *xy* maximum projections (**a, c**) and 5 μm *xz* projections (**b, d**) were captured in CX3CR1$^{gfp/+}$ (**a**), B6 (**b, d**), or LysM$^{gfp/+}$ (**c**) mice after compression injury (n=3, **a–c, e–g**; n=4, **d, h–i**). **a**, GSH pretreatment prevented jellyfish / honeycomb microglia formation (green) 1 hr following a compression injury that resulted in a cracked skull (blue). GSH administration also promoted survival of meningeal macrophages (green; white arrows). **b**, Relative to the vehicle control group, GSH pretreatment prevented glial limitans breakdown

observed 1 hr post-injury. SR101 (red) localizes above the glial limitans (white dotted line) in the GSH treated group. **c**, In GSH pretreated mice, no neutrophil response (green) to compression injury was observed at 6 hrs. **d**, GSH administered 15 min or 3 hrs post-compression injury significantly reduced parenchymal cell death observed at 12 hrs. PI^+ dead cells (red) reside primarily in the meninges of GSH-treated mice. (white dotted line = glial limitans). **e–g**, Bar graphs (mean±SD) show quantification of honeycomb / jellyfish microglia (**e**), glial limitans permeability (**f**), and neutrophil recruitment (**g**) in vehicle vs. GSH-treated mice following compression injury at the time points denoted above. **h**, The number of PI^+ dead cells per mm^3 (mean±SD) was quantified in the meninges at 30 min or 12 hrs post-compression injury. GSH significantly reduced meningeal cell death if applied before (pre-treatment), but not following (0 min, 15 min, 3 hrs) compression injury. P2X7 blockade increased meningeal cell death when administered 15 min after compression injury. **i**, Parenchymal cell death was quantified 12 hrs following compression injury in the denoted groups. All data in this figure are representative of three independent experiments, and asterisks denote a statistically significant difference ($p < 0.05$) from the vehicle control group.